

Supporting Information

Sn₄P₃/Sb Composite Electrodes as High-Performance Anodes for Li-Ion and Na-Ion Storages

Hiroyuki USUI,^{a,c,} Yasuhiro DOMI,^{a,c} Atsuki TERAMAE,^{b,c} Taisei KOHASHI,^{b,c}
Yuto SOHMA,^{b,c} Naoto OISHI,^{d,e} and Hiroki SAKAGUCHI^{a,c,*}*

^a *Department of Chemistry and Biotechnology, Graduate School of Engineering, Tottori University, 4-101 Minami, Koyama-cho, Tottori 680-8552, Japan*

^b *Course of Chemistry and Biotechnology, Department of Engineering, Graduate School of Sustainability Science, Tottori University, 4-101 Minami, Koyama-cho, Tottori 680-8552, Japan*

^c *Center for Research on Green Sustainable Chemistry, Tottori University, 4-101 Minami, Koyama-cho, Tottori 680-8552, Japan*

^d *School of Engineering Science, Kochi University of Technology, 185 Miyanokuchi, Tosayamada, Kami, Kochi 782-8502, Japan*

^e *Department of Social Design Engineering, National Institute of Technology, Kochi College, 200-1 Monobe, Nankoku, Kochi 783-8508, Japan*

*Corresponding Author:

Tel./Fax: +81-857-31-5234, +81-857-31-5265,

E-mail: usui@tottori-u.ac.jp, sakaguch@tottori-u.ac.jp

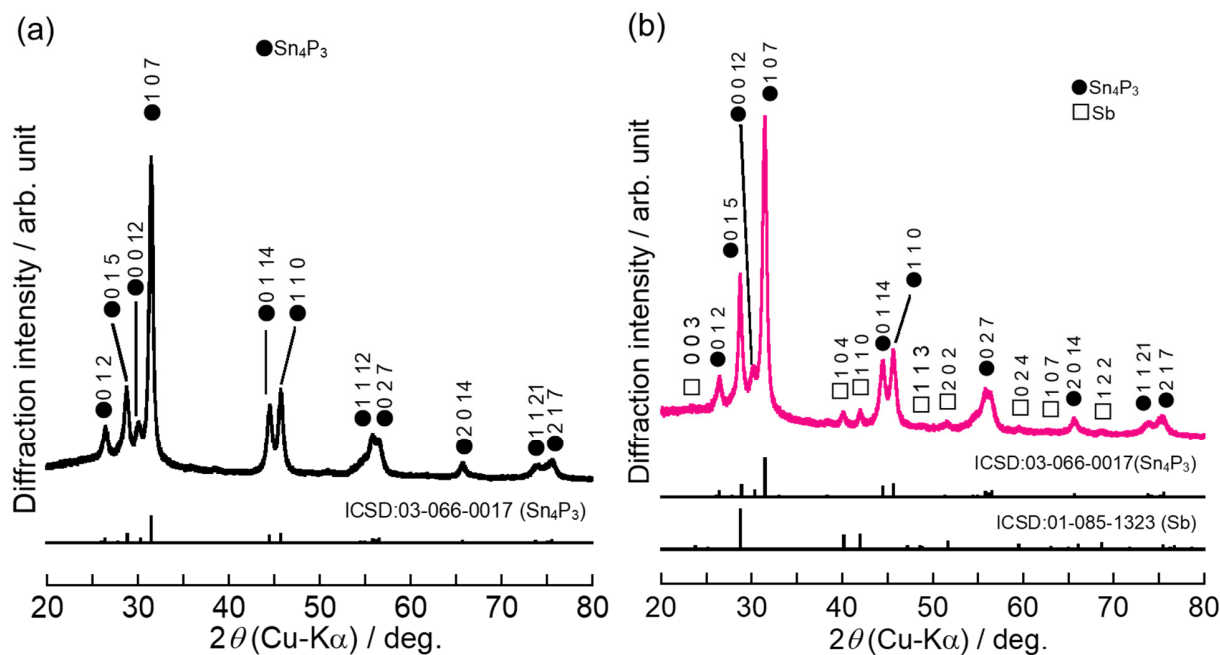


Figure S1 XRD patterns of active material powders composed of (a) Sn_4P_3 and (b) $\text{Sn}_4\text{P}_3/\text{Sb}$ (90:10 wt.%).

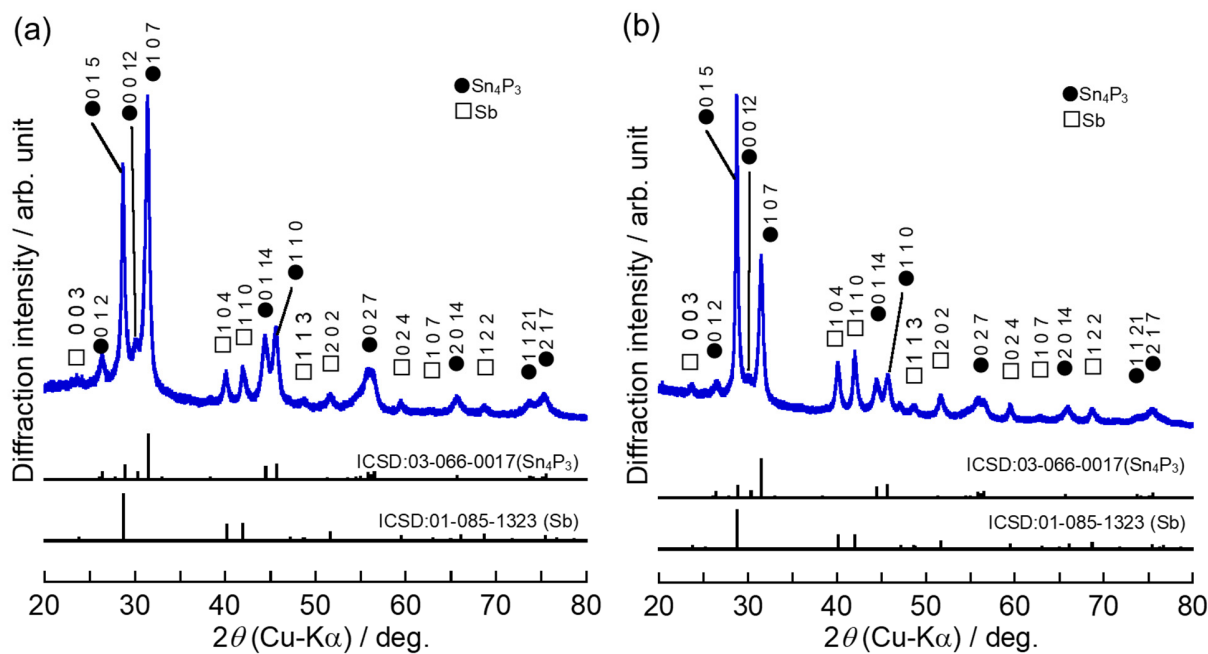


Figure S2 XRD patterns of active material powders composed of (a) $\text{Sn}_4\text{P}_3/\text{Sb}$ (80:20 wt.%) and (b) $\text{Sn}_4\text{P}_3/\text{Sb}$ (60:40 wt.%).

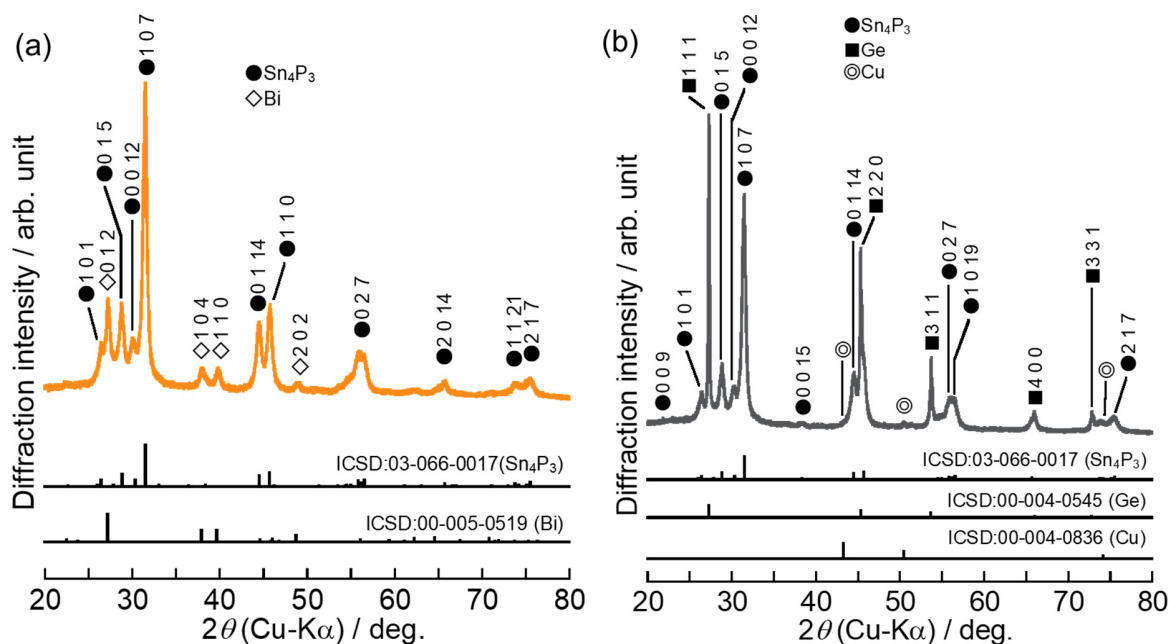


Figure S3 XRD patterns of active material powders composed of (a) $\text{Sn}_4\text{P}_3/\text{Bi}$ (70:30 wt.%) and (b) $\text{Sn}_4\text{P}_3/\text{Ge}$ (70:30 wt.%).

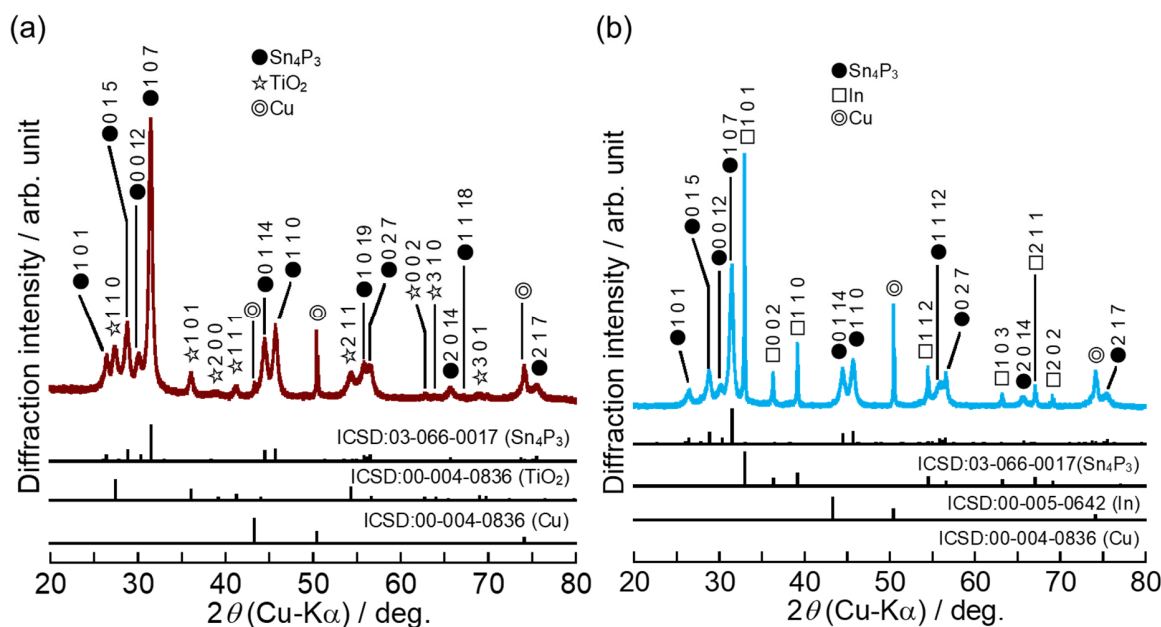


Figure S4 XRD patterns of active material powders composed of (a) $\text{Sn}_4\text{P}_3/\text{TiO}_2$ (70:30 wt.%) and (b) $\text{Sn}_4\text{P}_3/\text{In}$ (70:30 wt.%).

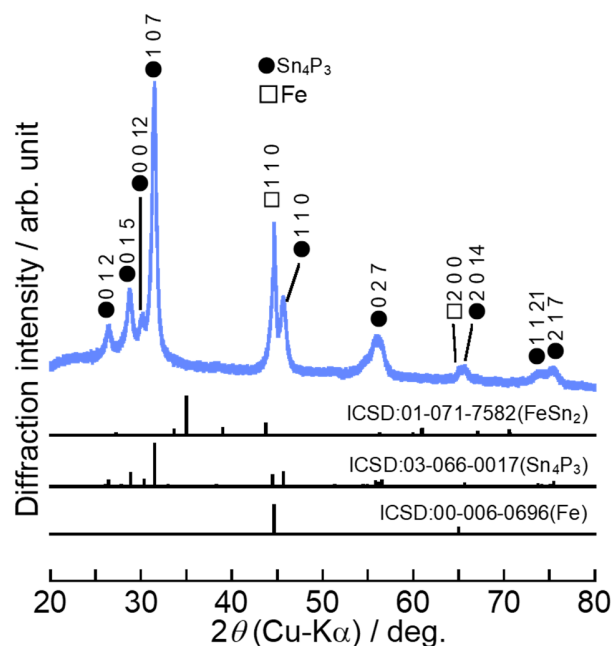


Figure S5 XRD pattern of active material powder composed of $\text{Sn}_4\text{P}_3/\text{Fe}$ (70:30 wt.%).

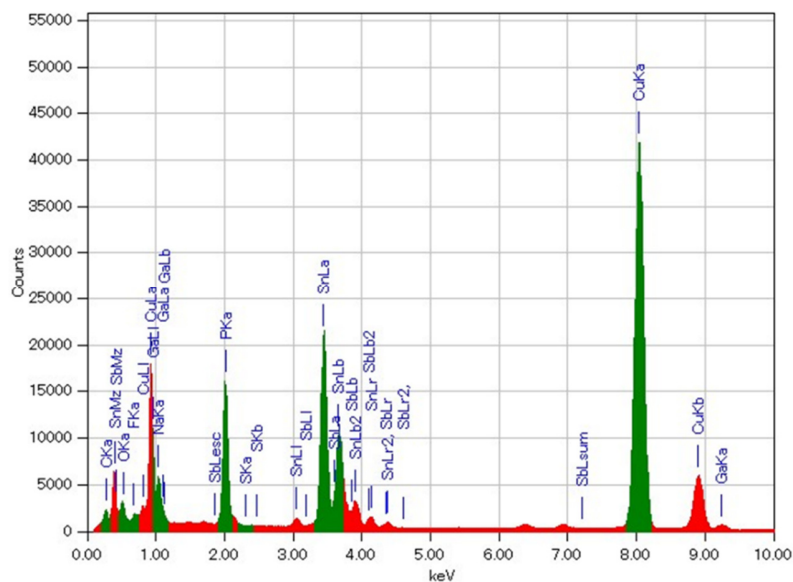


Figure S6 Result of energy dispersive X-ray spectroscopic analysis of $\text{Sn}_4\text{P}_3/\text{Sb}$ (85:15 wt.%) composite electrode at the full desodiation state after 50 cycles.

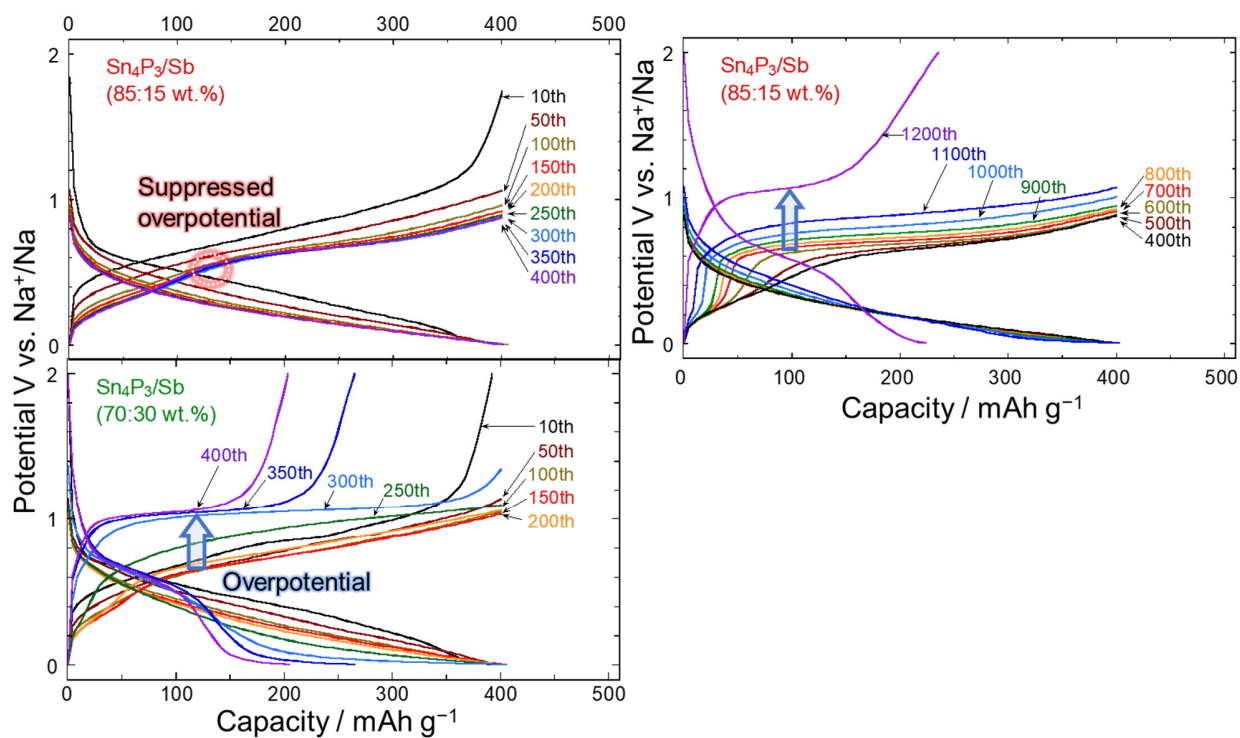


Figure S7 Charge-discharge curves of $\text{Sn}_4\text{P}_3/\text{Sb}(85:15 \text{ wt.}\%)$ and $\text{Sn}_4\text{P}_3/\text{Sb}(70:30 \text{ wt.}\%)$ electrodes as NIB anodes. The right figure shows the results of $\text{Sn}_4\text{P}_3/\text{Sb}(85:15 \text{ wt.}\%)$ electrode after 400 cycles.

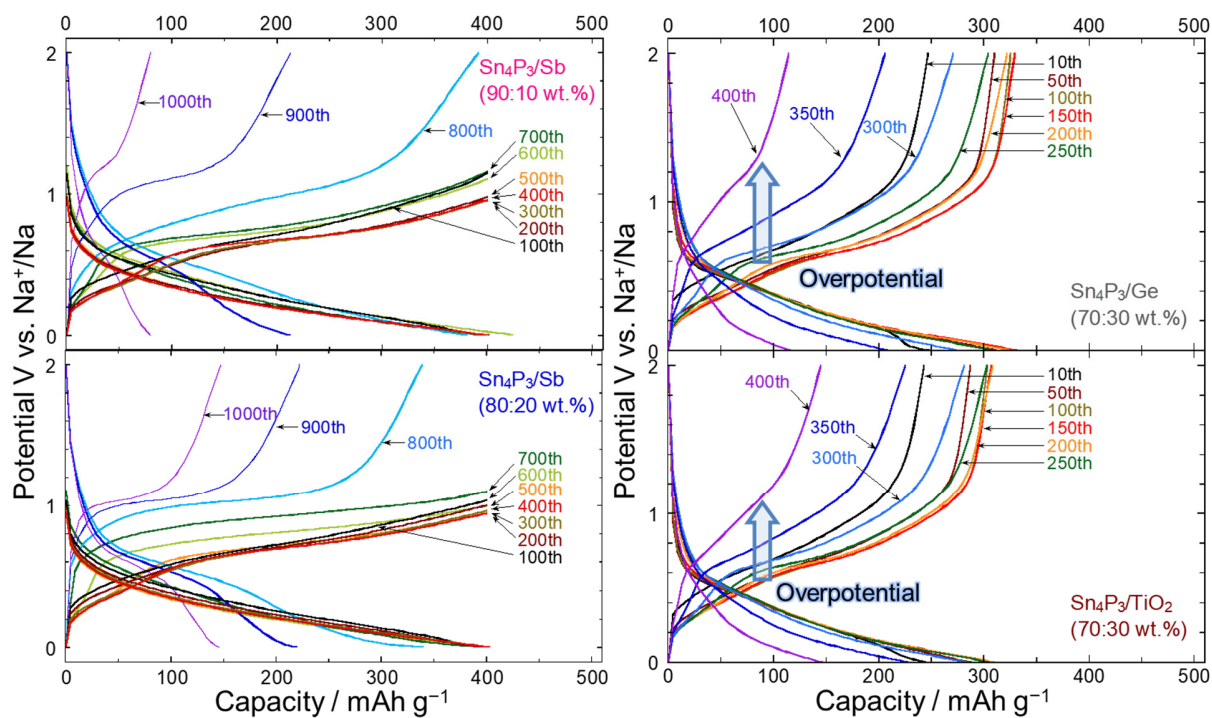


Figure S8 Charge-discharge curves of various composite electrodes of $\text{Sn}_4\text{P}_3/\text{Sb}(90:10 \text{ wt.}\%)$, $\text{Sn}_4\text{P}_3/\text{Sb}(80:20 \text{ wt.}\%)$, $\text{Sn}_4\text{P}_3/\text{Ge}(70:30 \text{ wt.}\%)$, and $\text{Sn}_4\text{P}_3/\text{TiO}_2(70:30 \text{ wt.}\%)$ evaluated as NIB anodes.

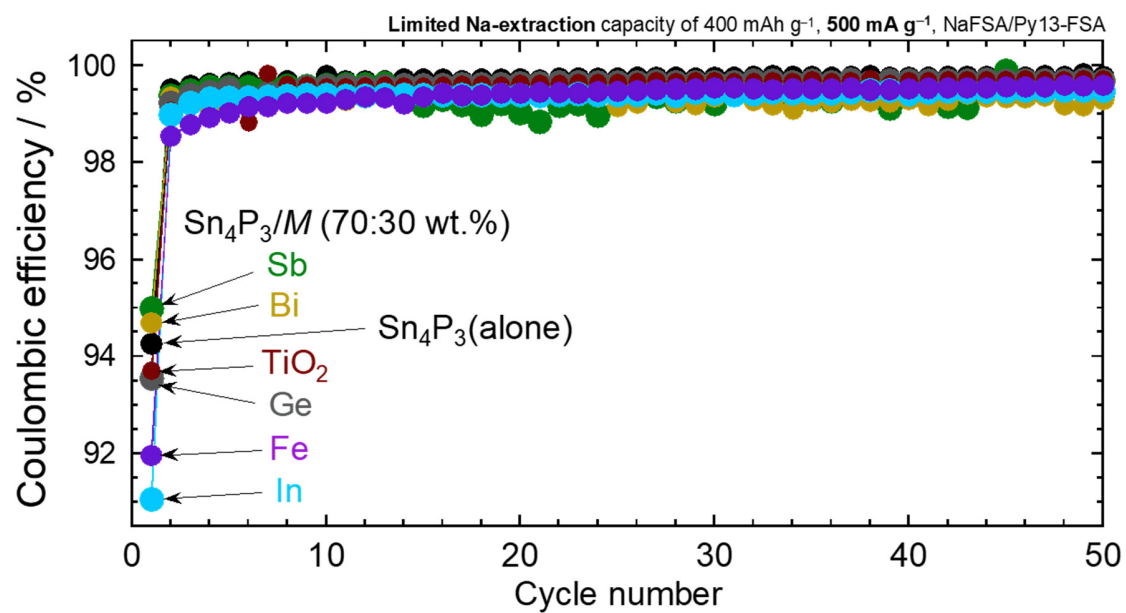


Figure S9 Coulombic efficiencies of Sn₄P₃/M composite electrodes evaluated as NIB anodes.

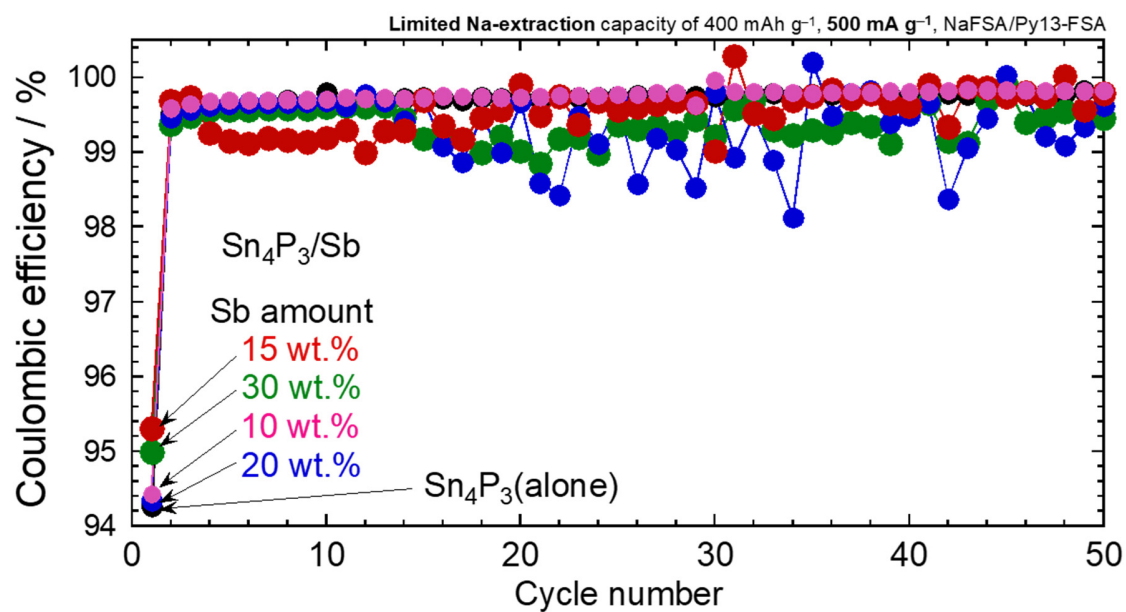
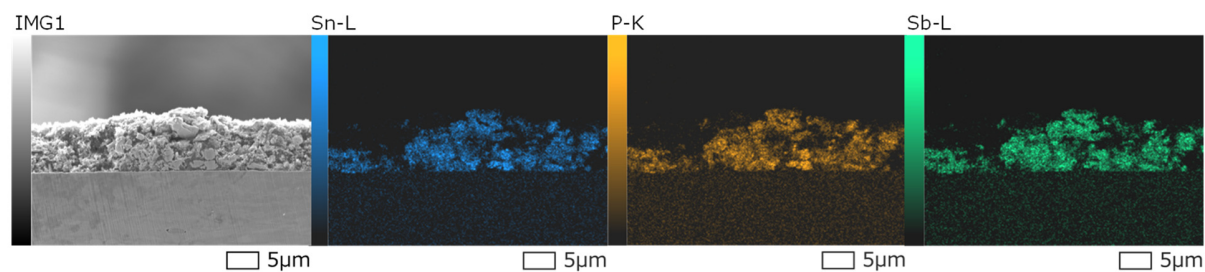


Figure S10 Coulombic efficiencies of Sn₄P₃/Sb composite electrodes with various Sb amounts as NIB anodes.

(a) Before cycling



(b) After 350 cycles

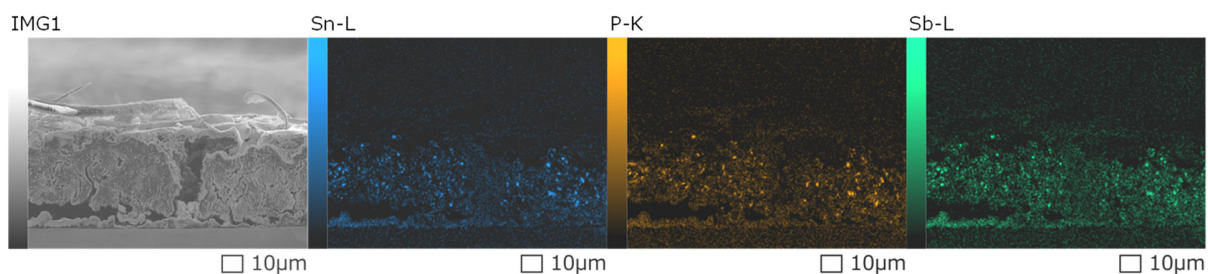


Figure S11 Results of energy dispersive spectroscopic analyses for cross-section of $\text{Sn}_4\text{P}_3/\text{Sb}(70:30 \text{ wt.}\%)$ electrodes (a) before cycling and (b) at the sodiation condition after 350 cycles.

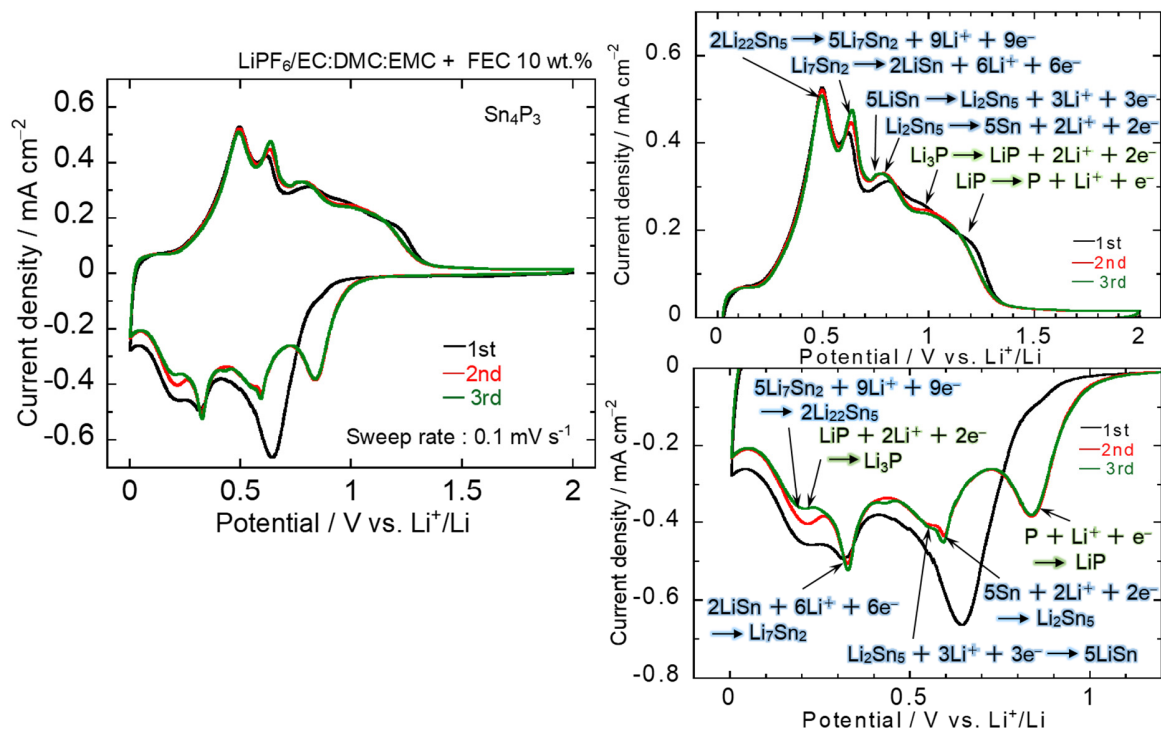


Figure S12 Cyclic voltammograms of Sn_4P_3 electrode evaluated as Li-ion battery anode.

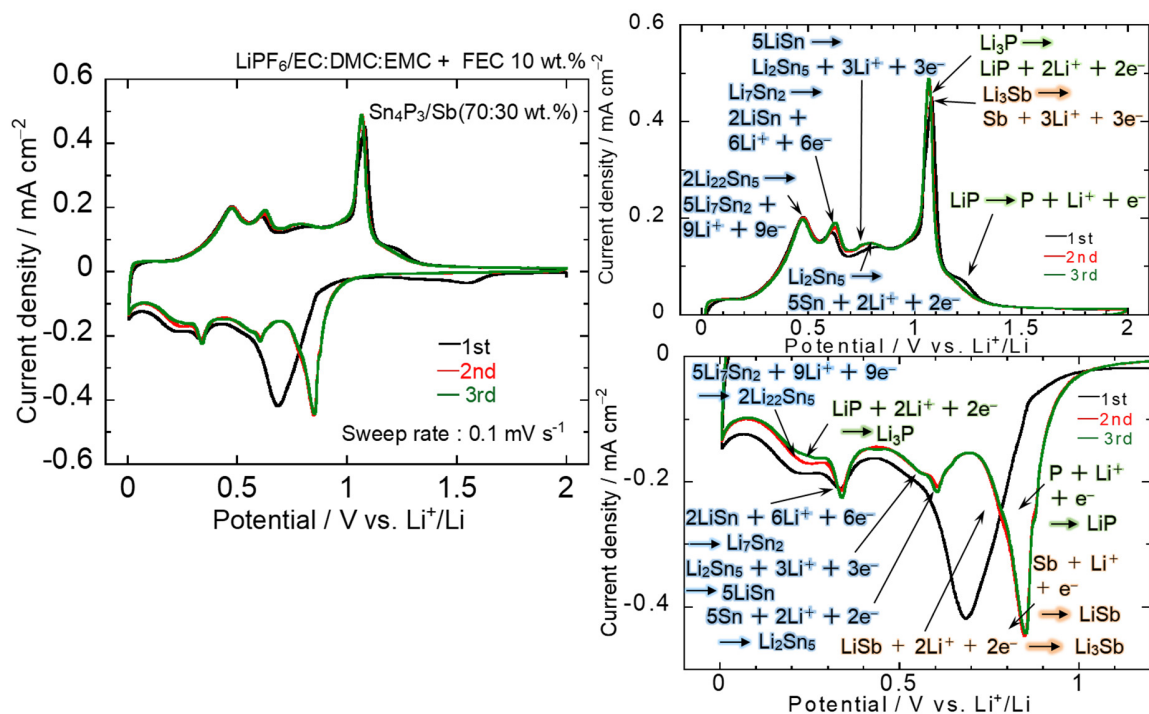


Figure S13 Cyclic voltammograms of $\text{Sn}_4\text{P}_3/\text{Sb}(70:30 \text{ wt.}\%)$ composite electrode evaluated as Li-ion battery anode.